Optical Materials: X 14 (2022) 100151

Contents lists available at ScienceDirect

Optical Materials: X

journal homepage: www.journals.elsevier.com/optical-materials-x

Detection of hidden oxygen interstitials in neutron-irradiated corundum crystals

A. Lushchik [a,**], V. Seeman [a], E. Shablonin [a], E. Vasil'chenko [a], V.N. Kuzovkov [b], E.A. Kotomin [b], A.I. Popov [b,*]

[a] Institute of Physics, University of Tartu, W. Ostwald Str. 1, 50411, Tartu, Estonia
[b] Institute of Solid State Physics, University of Latvia, Kengaraga 8, Riga LV, 1063, Latvia

A B S T R A C T

An α-Al_2O_3 (corundum) possesses unique optical, electrical and mechanical properties, demonstrates high tolerance to heavy irradiation and, in particular, is in a short list of candidates for optical/diagnostics windows in advanced fission and forthcoming fusion (DEMO) reactors. However, material functionality is strongly affected by structural defects induced by radiation of different types. Optical and magnetic characteristics of Frenkel defects (interstitial-vacancy pairs) as well as the processes of their thermal annealing (radiation damage recovery) have been investigated by means of optical absorption and the EPR methods in α-Al_2O_3 single crystals exposed to fast neutrons with fluence of 6.9×10^{18} n/cm^2. For the first time in metal oxides, a single oxygen interstitial, which is not adjacent to any other imperfection, has been detected. The analysis of the EPR spectra/parameters testifies that this interstitial forms with a regular oxygen ion a superoxide ion O_2^-, stabilized by a trapped hole. The interstitial becomes mobile above 500 K and recombines with a complementary oxygen vacancy that is a part of electronic F^+ or F centers. The thermal annealing kinetics of the F and F^+ centers has been theoretically analyzed in terms of interrelated diffusion-controlled recombination reactions of radiation defects. The analysis indicates that both, negatively charged and neutral oxygen interstitials (relevant absorption bands at 5.6 and 6.5 eV, respectively) co-exist in similar concentrations.

1. Introduction

Aluminium oxide, α-Al_2O_3 (corundum, sapphire, lattice structure belongs to space group $R\bar{3}c$ [1]) possesses fascinating mechanical, optical and electrical properties and, consequently, is widely used for technological applications in rather different areas. α-Al_2O_3 is applied as laser media (see, e.g. Refs. [2–4], and references therein); highly sensitive luminescent detectors of ionizing radiation (anion-deficient α-Al_2O_3 often named in literature as Al_2O_3:C) [5,6]; as cryogenic scintillation-phonon detector for dark matter as well as material in microelectronics, medicine and aerospace industry [7]. In addition, because of high resistance to heavy irradiation and low swelling even under exposure to fast neutrons with high fluences, single crystals and polycrystalline optical ceramics of α-Al_2O_3 are utilized as various components in fission-based energetics (moderators, coatings, waste disposal, absorbers, etc.) [8–10] and are in the list of promising functional materials in future advanced fission and deuterium-tritium fusion reactors (in particular, as optical/diagnostics windows in DEMO) [11–13].

By the modern concept, material radiation tolerance, in particular, the functionality of optical components, strongly depends on the accumulation of stable lattice defects, primary interstitial-vacancy Frenkel pairs and their aggregates. Just radiation-induced defects cause the appearance of selective absorption bands within transparency region of wide-gap materials (WGMs). For this reason, the creation mechanisms of radiation defects, processes of their accumulation and aggregation in various functional materials are of special importance. Note that the precise study of radiation damage recovery via the thermal annealing of initially irradiated crystals allows to estimate a real portion of the forming radiation defects able to survive at the real operating temperature of WGMs.

Experimental investigations of radiation processes in aluminium oxide exposed to irradiation by fast fission neutron, energetic electrons or swift heavy ions (SHIs) have been performed for a long time [8–10, 14–33]. It is generally accepted that elastic collisions of incident energetic particles with material nuclei/atoms are mainly responsible for radiation damage (formation of Frenkel pairs) in metal oxides. This displacement (impact, knock-on) mechanism solely describes the radiation damage under oxide irradiation by fast neutrons [8–10,34]. Note that the mechanisms of Frenkel defects creation, which are very efficient

* Corresponding author.
** Corresponding author.
E-mail addresses: aleksandr.lushchik@ut.ee (A. Lushchik), popov@latnet.lv (A.I. Popov).

https://doi.org/10.1016/j.omx.2022.100151
Received 31 December 2021; Accepted 21 April 2022
Available online 8 May 2022

in model alkali halides, namely, the decay of self-trapping excitons and recombination of totally relaxed conduction electrons with valence holes (see, e.g. Ref. [35], and references therein), are not employed in metal oxides for energetic reason. In contrast to majority of alkali halides, the formation energy of an interstitial-vacancy Frenkel pair in metal oxides significantly exceeds the energy gap E_g (in α-Al_2O_3, exciton absorption band and onset of band-to band electron transitions are located at around 8.8 and 9.4 eV, respectively [36]). Nevertheless, more complex ionization mechanisms (in particular, hot electron-hole recombination), to some extent, contribute also to defect creation in metal oxides exposed to SHIs that provide extremely high density of electronic excitations along ion tracks [30,37–41].

Optical characteristics (relevant absorption and emission bands) of oxygen-vacancy related Frenkel defects – the so-called F and F^+ centers (an anion vacancy with two or one trapped electron, respectively) [17,18,20–22,26,32] and their simplest aggregates, F_2 dimers in different charge states (two adjacent vacancies with two, three or four trapped electrons) [19–21,24,26,33] have been determined in corundum crystals. Because of paramagnetic origin of the F^+ center, the relevant signal of electron paramagnetic resonance (EPR) that contains hyperfine structure (HFS) due to the interaction of an unpaired electron with four aluminum nuclei surrounding the oxygen vacancy has also been revealed in a neutron-irradiated α-Al_2O_3 [16]. In addition, it was established long ago that the F-type point defects in additively colored (thermochemically reduced) corundum remain stable (immobile) up to about 1400 K [42], while the annealing of the F- and F_2-type defects in the irradiated α-Al_2O_3 samples occurs at significantly lower temperatures (~ 600-1000 K) due to their mutual recombination with becoming mobile oxygen interstitials – the complementary to anion vacancies Frenkel defects [19,21,24–27,31–33].

On the other hand, up to our recent study [32], a single oxygen interstitial remained the most hidden primary intrinsic lattice defect in metal oxides. Already in 1978, Halliburton and Kappers detected the EPR signal in irradiated MgO crystals, which was interpreted as an oxygen interstitial in a form of superoxide ion O_2^- and named as the H center [43]. Nevertheless, the analogy with an H center revealed earlier in alkali halides by the same EPR method (an interstitial halogen atom – a dihalide quasi-molecule X_2^- located at one anion cite [44]) was not complete, because O_2^- with spin $S = 1/2$ was initially localized nearby a cation vacancy. Since that time a set of similar paramagnetic superoxide ions was additionally detected in MgO [45,46], CaO [47–49], SrO [50], ZnO [45] and Na-β-Al_2O_3 [51], although in all these cases the O_2^- defect was not a single one but located adjacent to some structural defect or an impurity ion. Note that according to first principles calculations, single oxygen interstitials in MgO and α-Al_2O_3 undergo rapid transformation into dumbbell configuration and subsequent diffusion of neutral or charged (with respect to a regular lattice) interstitials has been theoretically analyzed as well [52–54]. Furthermore, the theoretical analysis of the thermal annealing kinetics of radiation-induced F-type defects in corundum in terms of bimolecular diffusion-controlled reactions with the participation of mobile interstitials has been performed also [31,55–57].

The present paper presents a brief review of our recent results on the detection/characterization of oxygen interstitials in fast-neutron-irradiated corundum single crystals. The manifestations of long-term uncatchable oxygen interstitials have been revealed by means of the EPR and optical absorption as well as via the theoretical analysis of the features of experimentally measured thermal annealing kinetics of anion Frenkel defects. The review is based on our recent publications [32,33,56,57] and relevant invited talk at the 11th International Conference on Luminescent Detectors and Transformers of Ionizing Radiation (Bydgoszcz, Poland, September 12–17, 2021).

2. Experimental

Single crystals of α-Al_2O_3 were grown by means of the Czochralski method by Union Carbide Corporation. These samples contained traces of paramagnetic trivalent Fe and Cr ions, the concentration of which was estimated by a special Bruker program as about 0.02 and 0.1 ppm, respectively. The crystal discs were irradiated by fast neutrons with energy of $E > 0.1$ MeV and the fluence of $\Phi = 6.9 \times 10^{18}$ n/cm^2 at the Oak Ridge National Laboratory, the irradiation temperature was up to 330 K. The neutron-irradiated samples for EPR and optical absorption measurements were cut off in the form of 7 × 7 mm^3 plates, both sides polished and parallel/perpendicular to the c crystal axes. The sample thickness varies from 3 mm (mainly for EPR measurements) down to 0.09 nm for some optical absorption measurements in order to remain within experimental limits of optical density (OD) value, OD ≤ 4.0.

The EPR study has been performed by means of a spectrometer Bruker ELEXSYS-II E500 (X-band and a field modulation frequency of 100 kHz). The angular dependences of the EPR line positions at the rotation of the magnetic field **B** around different crystallographic directions have been determined with a 1-5-degree step. In corundum, the a, b and c crystal axes – $[1\bar{2}10]$, $[10\bar{1}0]$ and [0001], respectively – are reasonable candidates for such directions. Note that the b axis is perpendicular to the c and a axes, whereas the b axis connects adjacent oxygen sites and the a axis lies along the bisectrix of oxygen triangles at the base crystallographic plane (as a result, there are three equivalent a and b axes). Varying microwave power P has been applied in order to separate the overlapping EPR spectra related to different paramagnetic centers. As is customary in literature, the derivative curves are presented as ordinates in figures with EPR spectra.

The spectra of optical absorption have been measured in a wide region up to near vacuum ultraviolet (VUV, up to about 8.5 eV in corundum) using a high-absorbance spectrometer JASCO V-660 (1.5-6.4 eV) and a home-made setup with a VUV-monochromator and the hydrogen discharge light source. The so-called radiation-induced optical absorption (RIOA) is obtained after subtraction of the absorption for a virgin (pristine) sample from the spectrum for the same sample after irradiation. Just selective RIOA bands are considered as a measure of relevant radiation defects.

The same stepwise annealing procedure has been applied in order to investigate temperature dependences of different radiation defect concentrations, which have been estimated via relevant RIOA bands or the EPR signal intensities. The irradiated sample was placed into a quartz reactor and heated to a certain temperature T_{pr} in a flowing argon atmosphere; kept at this T_{pr} for 10 min and then cooled down to room temperature (RT, reactor was extracted from the furnace). All EPR and RIOA spectra for the samples preheated with a sequential increase of T_{pr} were measured at RT. The same annealing procedure was successfully used in our studies of radiation damage recovery via the EPR and optical absorption methods in magnesium aluminate spinel crystals with different stoichiometry [58,59].

3. Theoretical

There exists a huge body of experimental kinetics of defect accumulation under irradiation and further thermal annealing (decrease in the defect concentration during heating), but theoretically and quantitatively these data were analyzed very poorly. The current level of analysis of material properties under prolonged irradiation is inadequate to the technological requirements for functional materials. In the last years, we proposed a new experimental-theoretical approach to comprehensive analysis of heavy radiation damage [31,55–57,60–63]. The essence of this approach is a set of chemical reactions describing the processes of recombination and mutual transformation of radiation defects. This set of the relevant kinetic differential equations is uniquely assigned to the defect complex. The quantitative correspondence of the

theory and experiment allows us to extract the desired kinetic parameters for the microscopic model. The fundamental results were obtained for the F and F^+ color centers and their complementary defects – interstitial oxygen ions as a function of radiation dose and temperature, with subsequent post-irradiation annealing, in a series of ionic solids: Al_2O_3, MgO and MgF_2 wide-gap insulators.

In this paper, new possibilities of the method are demonstrated on the basis of recent study of primary defect kinetics in corundum [56,57]. For the first time, the elaborated theory predicted the involvement of *two types* of mobile oxygen interstitials (charged H^- and neutral H^0) in their mutual recombination with complementary immobile oxygen-vacancy-containing centers (the F and F^+). The study revealed the key role of Coulomb interaction of charged complementary defects, the effects associated with the release of positive or negative charge in recombination processes, and also determined kinetic parameters such as diffusion activation energies and corresponding pre-exponents. The theoretical approach was described in detail in our recent paper [57], so we will not repeat the corresponding equations.

Note that the comparing of experiment and theory opens a unique opportunity to determine the fundamental material parameters. Therefore, before we proceed to the results, it is necessary to present the basic relations used for the interpretation of kinetic curves. We assume that the defect complex consists strictly of four types of Frenkel defects (two electronic defects F=F^0, F^+, and two types of interstitials, H^0, H^-). The recombination processes include four reactions (see Ref. [57] for more details). Each of the reactions, however, is diffusion-controlled, so the rates of all processes obey the well-known Smoluchowski equation [78–80]:

$$K = 4\pi DR\,, \tag{1}$$

where D is the coefficient of relative diffusion of the two reactants and R – recombination radius.

Note that the following experimental fact simplifies the theory. It is generally accepted that the electron-type and oxygen-vacancy-containing F and F^+ centers in corundum are immobile in the temperature range under consideration ($T < 1100$ K) [21,42]. Consequently, the reaction rates depend only on the diffusion coefficients of two types of mobile interstitials, $D_H^{(0)}$ and $D_H^{(-)}$. The diffusion coefficients exponentially depend on the temperature

$$D_H^{(-)}(T) \sim \exp(-E_a/k_BT),\ D_H^{(0)}(T) \sim \exp(-E_b/k_BT) \tag{2}$$

Since the activation energies for the migration of charged and neutral oxygen interstitials, E_a and E_b are rather different, we have two independent material parameters that determine diffusion (along with their pre-exponentials [57]).

For the reaction of neutral defects in solids, parameter R is of the order of lattice constant (10 Å). However, for the reaction of oppositely charged defects, the temperature dependence of the recombination radius should be considered according to Debye's relation [78,79,81].

$$R \sim \frac{T_c/T}{1-\exp(-T_c/T)} \tag{3}$$

Here we have introduced a characteristic temperature T_c (see definition, eq. (12) in Ref. [57]), which is expressed in terms of reagent charges, the dielectric constant of the medium and the recombination radius of neutral particles. The physical meaning of eq. (3) is very simple: at high temperatures (above the characteristic T_c), Coulomb effects can be neglected, the recombination radius practically does not differ from its value for neutral defects. In contrast, at low temperatures (below the characteristic T_c), the radii of recombination of charged and neutral defects may differ significantly. Our estimate [56,57] has shown that the characteristic temperature T_c for corundum is of the order of 1000 K. The temperature region where the experiment is carried out lies below the characteristic one. As a result, Coulomb effects are important and should be taken into account. Note, the characteristic temperature is very close to the upper temperature limit of the experiment and transients associated with switching on or off the Coulomb interaction can be detected.

The general problem of comparing theory and experiment, the fundamental possibility of extracting the values of material parameters from the experimental kinetics of defect annealing will be continued by us in paragraph *4.3*.

4. Results and discussion

4.1. EPR signal of oxygen interstitials

As it has already been mentioned in Introduction, the first report on experimental manifestations of a single oxygen interstitial in metal oxides is given in our recent paper [32]. Fig. 1 presents EPR spectra for this defect of a paramagnetic origin in a α-Al_2O_3 single crystal previously irradiated by fast fission neutrons. The spectra have been measured at RT, microwave power of $P = 0.6$ mW and orientations of the magnetic field **B** along three main crystallographic axes (*a*, *b* and *c*) of the corundum crystal as well as at arbitrary **B** orientation in a base plane (0001). A width of lines ascribed to a novel radiation defect (as will be proved below – a superoxide ion, hereafter the O_2^- center) is about 1.5-1.7 mT, while the number of relevant lines, from single one at **B** ||*c* to a triplet (the lowest spectrum), in a range of 342-352 mT obviously depends on the **B** orientation. The EPR lines marked by asterisk are related to still unidentified defects, which are not the subject of this study. A probe EPR signal (Cr^{3+} ions in a cubic MgO crystal) corresponds to a *g*-factor value of 1.9800 and helps to control the *g*-factor components for our novel defect.

To determine the orientation of the O_2^- center, it is necessary to measure the angular dependencies of the O_2^- line positions at the **B** rotation within different crystallographic planes. Fig. 2 demonstrates such dependencies at the **B** rotation in the base (0001) plane, i.e. around

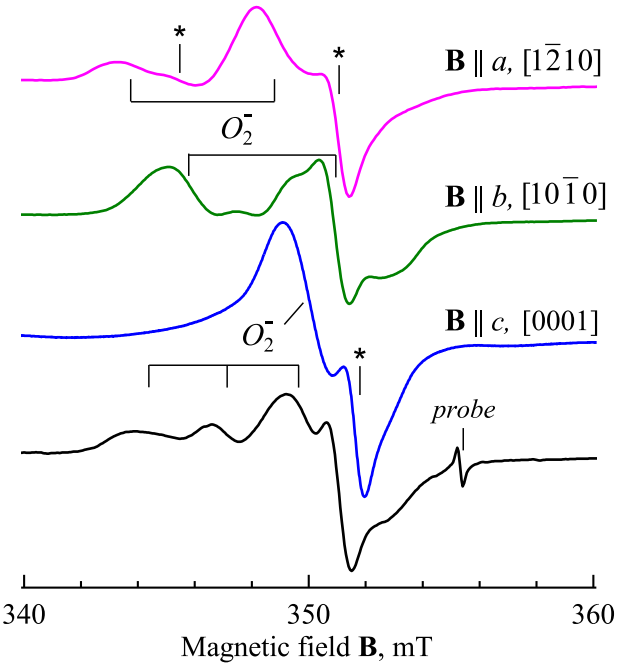

Fig. 1. EPR spectra measured at different orientation of **B** with respect to the *a*, *b* and *c* crystallographic axes of a neutron-irradiated α-Al_2O_3 crystal. The lowest spectrum is registered at $\varphi = 16°$ – an angle between **B** and the *a* axis (one of three equivalent *a* axes) in the (0001) base plane. Asterisks indicate signals of alien defects. Signal of a probe sample (Cr^{3+} in MgO) corresponds to $g = 1.9800$. $T = 295$K, $P = 0.6$ mW.

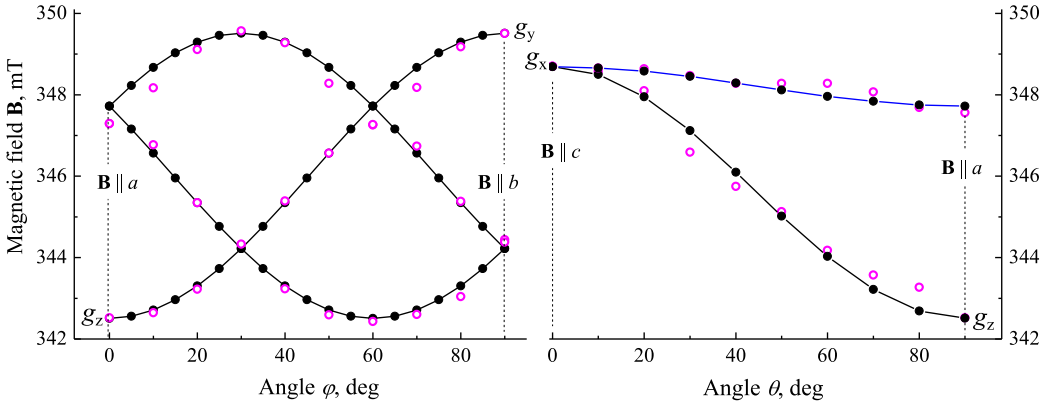

Fig. 2. The angular dependences of the O_2^- EPR line positions at the **B** rotation in the (0001) base plane (left, rotation around *c*) or the $(10\bar{1}0)$ plane (right, rotation around *b*) of a neutron-irradiated α-Al_2O_3 crystal. The angle φ is measured between the direction of the **B** and the axis *a*; the angle Θ – between the **B** and the axis *c*. Open circles – experimentally measured points, solid lines with filled circles – calculations. The orthogonal *x, y, z* axes of the O_2^- center (*g*-tensor) coincide with the *c*, *b* and *a* crystal axis, respectively.

the *c* axis (left part of figure) and in the $(10\bar{1}0)$ plane (rotation around the *b* axis, right figure part). Open symbols correspond to experimentally measured points, while solid lines with filled symbols represent the results of calculations performed using the relevant formula from Ref. [64] or via EasySpin program [65].

There is a clear correlation of angular dependencies with the EPR spectra presented in Fig. 1. At arbitrary **B** direction in the base plane, the EPR spectrum of the O_2^- center consists of three lines with comparable peak intensities, while two lines are converged at **B** || *a* or **B** ||*b* and reach extremum positions if **B** coincides with the *a* ($\varphi = 0°$, $g_z = 2.0459$) and the *b* axis ($\varphi = 90°$, $g_y = 2.0049$), respectively. When **B** is rotated around the *b* axis (right part of Fig. 2), a single line at $g_x = 2.0096$ ($\Theta = 0°$) splits into two components with the maximum interline distance at **B** || *a* and extremum positions at $g_z = 2.0459$ and $g = 2.016$, respectively. Unfortunately, we have not succeeded in precise measuring the angular dependences for the O_2^- center at the **B** rotation around the *a* axis because of partial overlapping with the EPR lines related to other defects. Note that in all cases presented there is rather nice fit of the experiment with the calculated curves of angular dependencies.

Based on the above-mentioned data from angular dependences we can conclude that the *z* and *y* axes of the *g* tensor both lie in the (0001) plane, whereas the *z* axis is parallel to the *a* crystal axis and *x* ||*c*. The principal values of the *g* tensor components are determined as follows: $g_z = 2.0459$, $g_y = 2.0049$ and $g_x = 2.0096$. A standard formula, $h\nu = g\,\mu_B B$ (μ_B – Bohr magneton) allows to determine these experimental values from the EPR spectra. Therefore, the orientation of the paramagnetic O_2^- center is along the *a* axis (there are three equivalent *a* axes), i.e. along a bisectrix of an oxygen triangle at the base corundum plane. What is even more important, a complete coincidence of the paramagnetic center axis with *a* confirms that there is no any other structural imperfection/defect in the immediate vicinity of the O_2^-. Otherwise, the molecular axis of the O_2^- center should be declined.

If at a certain **B** direction, the EPR spectrum consists of only one line (see Figs. 1 and 2), the relevant paramagnetic center possesses spin of $S = 1/2$. A positive shift of the *g*-factor parameters from the free electron *g*-factor ($g_e = 2.0023$) testifies a hole origin of our paramagnetic center. At the same time, in general, a hole could be localized at an oxygen in a regular lattice site or belong to a molecular-type oxygen defect. In the first case we deal with so-called *V*-type trapped-hole EPR-active defects – a hole trapped at regular anion site in a form of O^- next to some structural/impurity defect. Such *V*-type trapped-hole defects have thoroughly been studied in Al_2O_3 [66–69] and MgO [69–71] crystals and relevant values of the g-factor components have been determined. In particular, the so-called O^-V_{Al} center (O^- adjacent to an aluminum vacancy) was detected in neutron- and gamma-irradiated or even especially treated α-Al_2O_3 crystals [14,15,66–69]. However, we have not detected these O^-V_{Al} centers in our α-Al_2O_3 samples ($\Phi = 6.9 \times 10^{18}$ n/cm^2), tentatively, due to more efficient creation of the O_2^-. Note that a typical ratio between the *g* tensor components, $g_y \approx g_x > g_z$ and rather low maximum value of $g = 2.020$ is valid for all *V* centers in corundum and MgO.

On the other hand, based on the literature data [45–51], another ratio between the *g* tensor components, namely $g_z > g_y \approx g_x$ is typical for a set of the O_2^- molecules definitely associated with some other imperfection in a number of metal oxides (Na-β-Al_2O_3, MgO, CaO, SrO, ZnO). More specifically, the values of two components are close and significantly lower than that for the g_z one (from $g_z = 2.059$ in Na-β-Al_2O_3 to $g_z = 2.066$ in MgO, see for details Table in Ref. [32]). The g_z, g_y and g_x values for the O_2^- center detected in our neutron-irradiated α-Al_2O_3 single crystals fit with those for the "imperfection-associated" O_2^- molecules in the above-mentioned metal oxides, and the maximum value of $g = 2.0459$ for the single (isolated) O_2^- center in corundum significantly exceeds that for a set of the *V*-type centers. In addition, the thermal decay of the O^-V_{Al} center via a hole release takes place at relatively low temperatures, 370-530 K [67,68], while the thermal stability of the O_2^- center under consideration is significantly higher (see next Section).

It is worth noting that, in contrast to the case of the F^+ center [16], the EPR spectrum of the O_2^- center registered at any temperature down to 5 K does not demonstrate HFS due to a hole interaction with four neighbor Al^{3+} ions. First of all, the center is composed of oxygen, whereas only negligible amount of oxygen nuclei (rare ^{17}O isotope) have a nonzero magnetic moment; and, secondly, the EPR lines of the O_2^- center are rather wide, thus, hampering the resolution of HFS if any.

Summarizing this Section, the analysis of the EPR data confirm that a hole-type paramagnetic defect with $S = 1/2$, a kind of an oxygen interstitial has been experimentally revealed in neutron-irradiated α-Al_2O_3, for the first time in metal oxides. The radiation-induced O_2^- molecule is the result of an interstitial interaction with a regular oxygen, and the resulting dumbbell configuration is stabilized by a trapped hole. The O_2^- superoxide ion occupies only one regular site in the (0001) base plane, is oriented along a bisectrix of the oxygen triangle (i.e. along equivalent *a* axes), and is not adjacent to any additional structural defect. The concentration of the O_2^- and F^+ centers in our irradiated Al_2O_3 crystal is practically the same and according to a special Bruker program is determined as about 1×10^{18} cm^{-3}.

It should be pointed out that the experimentally established superoxide defect configuration was completely confirmed by relevant density functional theory calculations using the state-of-the-art hybrid

exchange-correlation functionals (the detailed description of these DFT calculations is presented in Ref. 32).

4.2. Annealing of neutron-induced defects, optical characteristics of oxygen interstitials

Additional proofs of the suggested microstructure of the O_2^- center that contains an oxygen interstitial can be obtained via the study of radiation damage recovery at a subsequent thermal annealing of the neutron-irradiated corundum crystal. It is worth noting, that the radiation-induced origin of a certain structural defect can be confirmed by irreversible annealing of its quantitative characteristics (EPR signal intensity or relevant band of optical absorption, more appropriately – RIOA band, see Experimental section). Additional exposure of totally annealed corundum sample to X-rays at RT can provide, due to energetic reasons, only recharging of impurities and as-grown structural defects. The energy released at the recombination of the forming electron-hole pairs is insufficient for the creation of a Frenkel (interstitial-vacancy) pair, and the reappearance of the EPR signal or RIOA band related to a certain type of defects, which were created at initial irradiation by fast neutrons, is not possible. Looking ahead, the O_2^- centers in our neutron-irradiated crystals are typical intrinsic radiation-induced structural defects.

Of particular interest is the correlation between the paramagnetic O_2^- centers and a relevant RIOA band in our neutron-irradiated α-Al_2O_3 single crystals. Fig. 3 shows the RIOA spectrum measured at RT in a wide region, from 1.5 eV up to near-VUV (~8.5 eV) for an irradiated α-Al_2O_3 sample ($\Phi = 6.9 \times 10^{18}$ n/cm^2). The spectrum consists of two groups of pronounced RIOA bands, above and below 4.5 eV, the origin of which was thoroughly studied and considered in the literature. Three low-energy bands peaked at about 2.75, 3.45 and 4.1 eV are ascribed to the simplest aggregates of the *F* centers, two adjacent oxygen vacancies – F_2 dimers in different charge states with respect to a regular lattice [19–21,24,26,33]. These F_2^{2+}, F_2^+ and F_2 color centers contain two, three and four trapped electrons, respectively. However, the main objects of the present study are high-energy peaks, a part of which are definitely related to single oxygen vacancies in a form of the *F* (RIOA band with the maximum at 6.07 eV) and F^+ centers (bands peaked at 4.8 and 5.3 eV) [17–21,24,26,31–34].

There is evident overlapping of the absorption bands of different origin. Nevertheless, the selective contribution of a certain-type Frenkel defects to the RIOA can be analyzed via decomposition of the RIOA spectrum into elementary components, Gaussians (see Fig. 4*a*). The estimation of defect concentration is based on the characteristics of the elementary Gaussian (peak intensity or integral) responsible for the defects of a certain type. It has already been mentioned that the initial concentration of the ERR-active F^+ centers in our irradiated samples is equal to 1×10^{18} cm^{-3}, this value is also confirmed by the Smakula-Dexter formula for the corresponding RIOA bands.

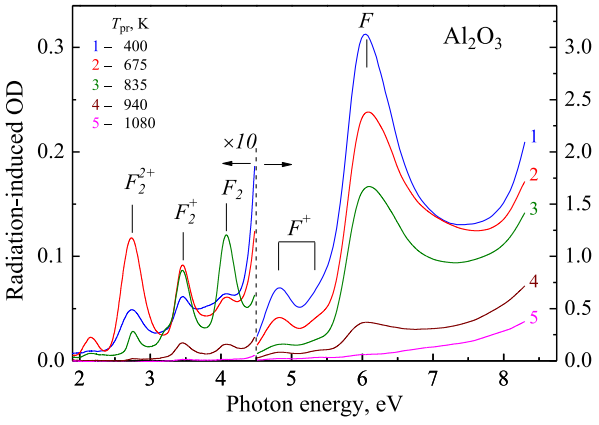

Fig. 3. The spectra of RIOA measured at RT for an Al_2O_3 single crystal irradiated with fast neutrons ($\Phi = 6.9 \times 10^{18}$ cm^{-2}, curve 1) or additionally preheated to different temperatures T_{pr} (curves 2 to 5). The sample thickness equals $d = 0.09$ mm. Two different scales are used for optical density values below and above 4.5 eV. The spectra after irradiation and preheating to $T_{pr} =$ 400 K coincide with each other.

The same decomposition procedure was performed for all RIOA spectra measured after preheating of the neutron-irradiated crystal to various temperatures T_{pr}. Sequent preheatings were executed at the same conditions with stepwise growing T_{pr}. The examples of these RIOA spectra, all measured at RT, and their decompositions into elementary Gaussians are presented in Figs. 3 and 4. Note, that the spectra after irradiation and preheating to $T_{pr} = 400$ K coincide with each other (irradiation was performed long ago at increased temperature, up to 330 K). A set of the RIOA spectra measured after each $T_{pr} = 300$-1150 K and decomposed into the same elementary components allowed us to construct temperature dependences for the concentration of different radiation defects.

The upper part of Fig. 5 presents such normalized annealing curves for the single *F* and F^+ centers as well as radiation defects responsible for the Gaussian component peaked at 5.6 eV. The results of the EPR signal pulse annealing for the paramagnetic O_2^- and F^+ centers are shown in Fig. 5*b*. In both cases, the EPR and optical measurements, exactly the same annealing procedure was used. The analysis of the presented experimental results leads to a number of conclusions.

Firstly, a temperature dependence of the F^+ concentration does not depend on Gaussian peak (at 4.81 or 5.33 eV) used for its estimation, parameters of these elementary Gaussians remain the same in the irradiated samples with different thickness which indicates that this is the same defect. Secondly, the annealing curves for the F^+ centers nicely coincide, regardless of whether the defect concentration is estimated by the EPR signal or the integral of a relevant RIOA Gaussian. Such excellent correlation between the EPR and optical characteristics of the same defects in different metal oxides was already reported in the literature (see, e.g. Refs. [32,58,59,63]). Accordingly, the RIOA Gaussian at 5.6 eV in a neutron-irradiated α-Al_2O_3 can be ascribed to the EPR-active O_2^- centers. Thirdly, in contrast to many other metal oxides (for MgO and magnesium aluminate spinel see our previous studies [62,63]), the thermal annealing of the *F* and F^+ centers is a multistage process (note a pronounced step around 750 K) and, what is even more important, there is an obvious high-temperature shift for the *F*-decay. These features of the *F* and F^+ annealing will be thoroughly analyzed in the next Section. However, before we want to draw attention to some other circumstances.

First, radiation-induced formation of two types of the electronic *F* and F^+ centers hints on the existence of two complementary interstitials – neutral and negatively charged oxygen interstitials (hereafter called H^- and H^0). The first one is involved in the formation of the O_2^- defect discussed above, while another, the H^0 interstitial we associate with the optical absorption band at 6.5 eV, on the basis of the annealing kinetics of the *F*-type and other centers discussed below.

In model alkali halides, complicated (multistage) annealing process for anion Frenkel defects (so-called *α-I* and *F–H* pairs) was explained by different mobility of halide interstitials (charged ions – *I* centers, and neutral atoms – *H* centers), which after becoming mobile participate in mutual recombination with complementary Frenkel defects, still immobile charged and neutral anion vacancies (*α* and *F* center, respectively) [35,44,72–75]. In metal oxides (including corundum), the thermal annealing of radiation-induced *F* and F^+ vacancy-containing centers is also caused by their recombination with complementary mobile oxygen interstitials [19,21,24–27,31–33]. According to Fig. 5*b*, the annealing of the O_2^- centers is completed to about 750 K, while the main decay occurs at slightly lower temperatures than the first annealing stage of the F^+ centers (where decay roughly two thirds of the F^+). On

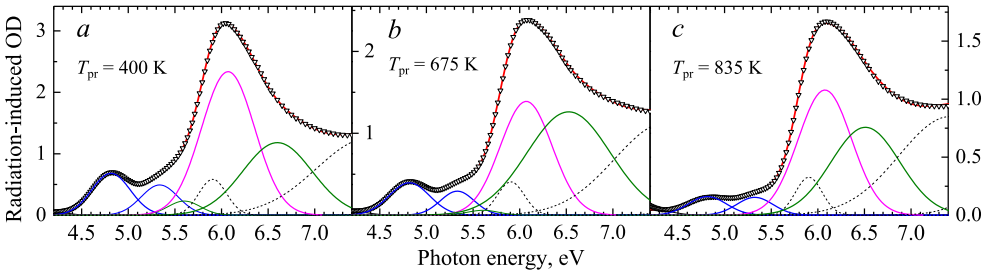

Fig. 4. Spectra of RIOA and their decomposition into Gaussian components for an α-Al_2O_3 single crystal (d = 0.09 mm) after irradiation by fast neutrons ($\Phi = 6.9 \times 10^{18}$ cm^{-2}, part *a*) or additional preheating of the irradiated crystal to T_{pr} = 675 K (part *b*) and T_{pr} = 835 K (part *c*). Symbols represent experimental points, solid red line – a sum of Gaussian components. All spectra were measured at RT. The spectra after irradiation and preheating to T_{pr} = 400 K coincide with each other, note that OD scales are different. (For interpretation of the references to color in this figure legend, the reader is referred to the Web version of this article.)

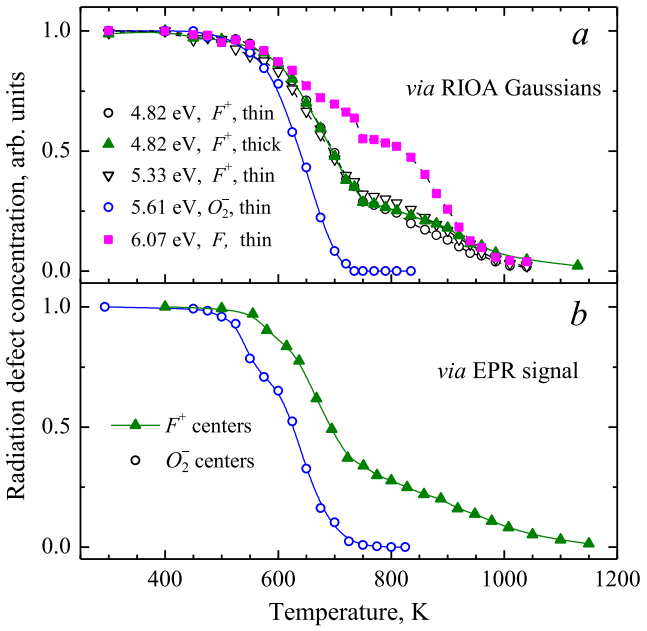

Fig. 5. The normalized annealing kinetics of the F, F^+ and O_2^- centers in an Al_2O_3 single crystal irradiated with fast neutrons (6.9×10^{18} cm^{-2}, RT). Defect concentration is estimated via integral of RIOA Gaussian (part *a*) or the EPR signal (part *b*). Maximum location of the Gaussian related to a certain defect and sample thickness (thin sample of 0.09 mm, thick – 0.37 mm) are specified in figure legend.

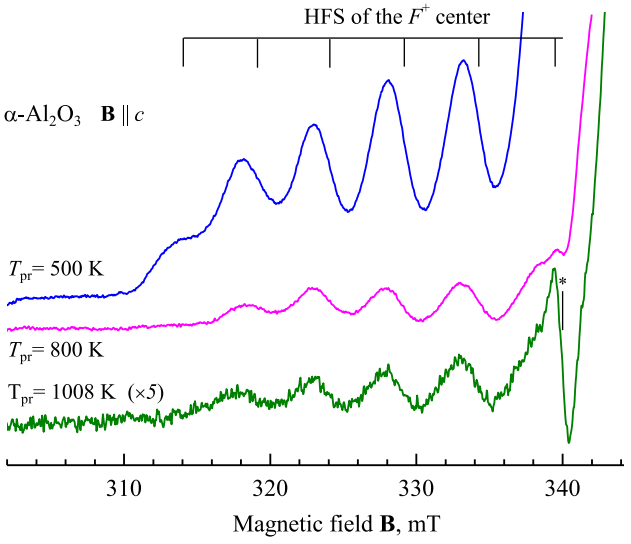

Fig. 6. A low-field part of EPR spectra of the F^+ center for a neutron-irradiated Al_2O_3 crystal additionally preheated to 500 K, 800 K and 1008 K. The spectra are measured at RT, **B** direction parallel to the *c* axis and P = 0.1 mW. The intensity of the lowest spectrum is multiplied by a factor of 5. Asterisk indicates signal of an alien defect.

the other hand, the annealing of neutral F centers needs even higher temperatures. Therefore, the oxygen interstitial related to the O_2^- center (with RIOA Gaussian at 5.6 eV and complementary to the F^+) should be a charged one (the H^- center). The shift in annealing of the EPR signals of the O_2^- and F^+ just reflects the release of the H^- incorporated in a molecular-type O_2^- center (first stage causing already the decay of EPR signal) and subsequent migration towards immobile F^+ center and recombination with it (this second stage requires additional time).

In general, the *F*-type centers from a long high-temperature tail in the annealing curves could be additionally associated with some impurity ions. In alkali halides, the optical characteristics of the *F* centers, single ones and associated with impurity ions or impurity-vacancy dipoles clearly differ [73,74]. Fig. 6 presents low-field parts of EPR spectra of the F^+ center for a neutron-irradiated Al_2O_3 crystal additionally preheated to 500 K, 800 K and 1008 K. It is clearly seen that HFS is exactly the same and the F^+ centers involved in a mutual recombination with mobile interstitials have the same microstructure within a whole temperature scale. As it was mentioned in Experimental Section, the concentration of impurities in our samples is rather low and a dominant part of the F^+ (as well as *F*) centers are formed in regular lattice regions. In addition, temperature-prolonged annealing kinetics mainly reflects the involvement of several types of interstitials starting to migrate at different temperatures.

Note that the pairs of the F^+ centers with total spin S = 1 have been already detected by the EPR method in cubic CaO and MgO single crystals irradiated by fast neutrons [76,77]. According to our preliminary data, EPR signal of such F^+-F^+ pairs (i.e. F_2^{2+} dimers with typical RIOA band peaked at 2.75 eV) has been detected as well. However, these results are beyond the scope of the present study and will be presented in a separate paper.

4.3. *The recombination kinetics of oxygen Frenkel defects*

In this Section, we discuss a qualitative problem: how strongly the defect annealing kinetics depend on a choice of defect parameters and initial conditions (defect concentrations before annealing) or how unique is the choice of theoretical parameters in the analysis of experimental data on defect annealing.

We start with Fig. 7 (see also [56]) which shows the results of theoretical fitting to the experimental annealing of elementary absorption bands for the following four-defect complex: 4.81 eV (F^+), 6.07 eV ($F \equiv F^0$), 5.60 eV (H^-) and 6.53 eV (H^0) using the least square method.

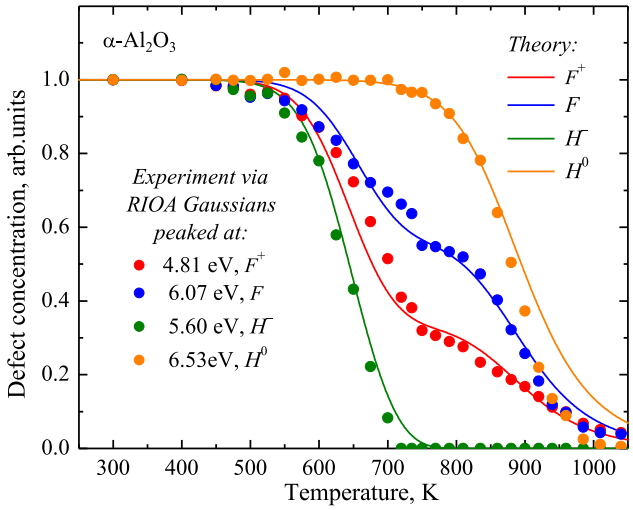

Fig. 7. The normalized experimental annealing kinetics (symbols) for four types of primary defects and their theoretical analysis (solid lines). Note the gap between the F and F^+ curves.

We already concluded [56] that the fraction of the charged Frenkel pairs constitute 55% of the total initial concentration of defects ($w^+ = 0.55$), i. e. neutral and charged defects are produced under neutron irradiation in nearly equal concentrations. Theoretical fitting for migration energies for charged and neutral interstitials ($E_a = 0.8$ and $E_b = 1.2$ eV, respectively) coincide with independent quantum-chemical calculations [53, 54]. We also found two relevant pre-exponentials, $X_a = 2 \times 10^3$ K^{-1} and $X_b = 2 \times 10^4$ K^{-1}. The corresponding definitions are given in our previous work (eqs. (21) and (22) in Ref. [57]), but we will not discuss the meaning of these less important factors. We took also into account the Coulomb interactions between the oppositely charged F^+ and H^- defects and estimated $T_c = 1000$ K. (eq. (3)).

A series of Fig. 8*a-c* demonstrates how the calculated annealing kinetic curves depend on the initial conditions and defect parameters. In Fig. 8*a*, we use the same E_b, X_a, X_b, w^+ parameters as in summarizing Fig. 7 but neglect the Coulomb interaction ($T_c = 0$) and increase the migration energy of H^- centers from $E_a = 0.70$ eV (solid line) to $E_a = 0.80$ eV (dashed line) or $E_a = 0.90$ eV (dash-dotted line). Also, as one can see, the migration energy E_a defines the temperature where the H^- concentration starts to decay but does not influence the shape of the annealing curves (cf. curves 1, 1′ and 1″). Moreover, the E_a does not affect the annealing kinetics of the neutral interstitials (curves 3, 3′, 3″ overlap). A similar conclusion can be done about the variation of E_b with fixed E_a. As a result, the search for the optimal migration energy of a charged interstitial is simplified: the curve 1′ with $E_a = 0.80$ eV turns to be the closest to the experimental data (green points). In a similar way, the optimal value for neutral interstitials is $E_b = 1.20$ eV. Both the optimized migration energies coincide with the ones predicted by the quantum-chemical calculations [53,54].

The neglect of the relatively weak Coulomb interactions, $T_c = 0$ K, results in the overlap of the F and F^+ curves which simplifies the preliminary analysis. Their annealing curves upon E_a variation (curves 2, 2′, 2″) always lie between those for the charged and neutral interstitials – in agreement with the experiment (see Fig. 7). Moreover, the F centers show a step in the annealing curve around 750 K. Based on Fig. 8*a* we conclude that such step arises only if the migration energies for charged and neutral interstitials considerably differ: in particular, compare curves with a visible step (curve 2), a small one (2′), and curve 2″ without a step. In other words, the step gives us additional hint about the choice for the migration energies.

All the above said is valid for the fixed fraction of the parameter w^+=

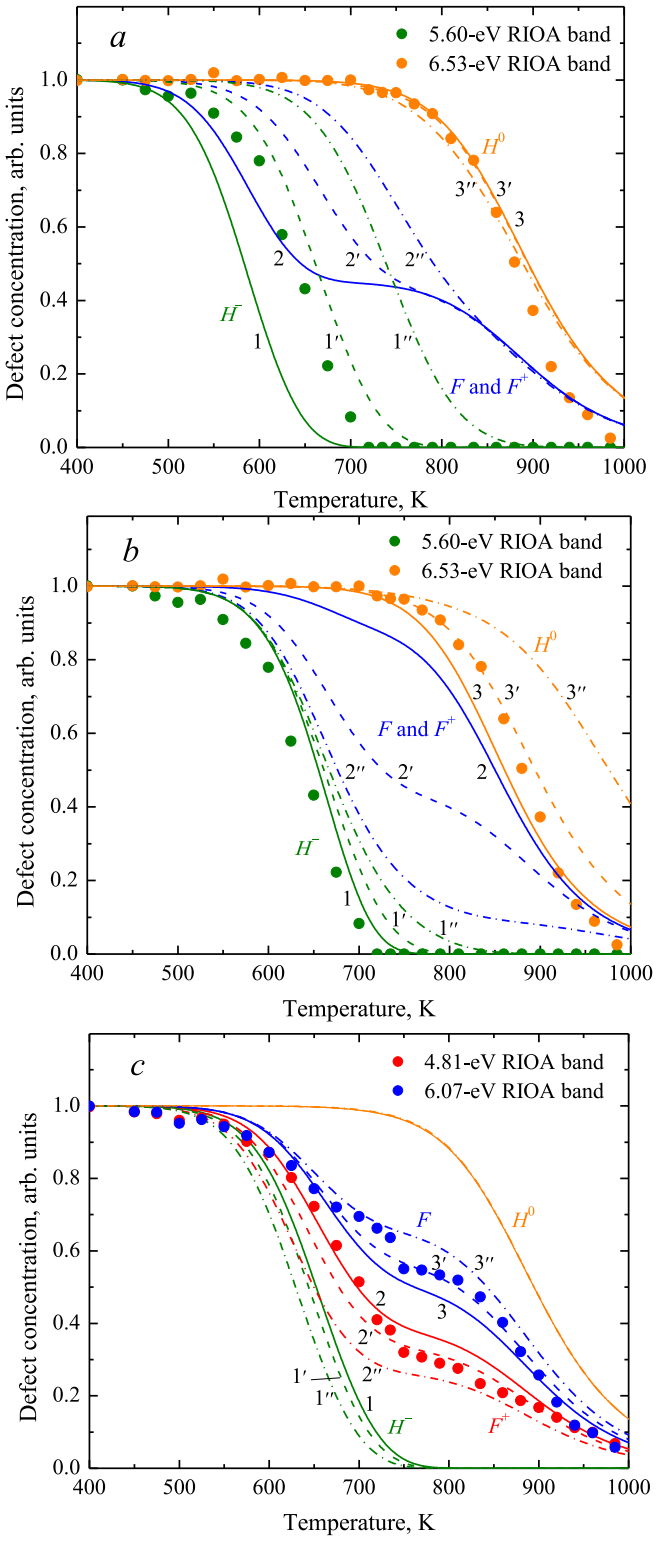

Fig. 8. The fitting of calculated annealing kinetic curves for different defects to experimental ones (symbols are related to different RIOA Gaussians) by varying the interstitial migration energies E_a (part *a*), fraction of charged defects w^+ (*b*) and characteristic temperature T_c (*c*).
Solid lines correspond to $E_a = 0.70$ eV, $w^+ = 0.10$ and $T_c = 500$ K; dashed lines – $E_a = 0.80$ eV, $w^+ = 0.55$ and $T_c = 1000$ K; dash-dotted lines – $E_a = 0.90$ eV, $w^+ = 0.90$ and $T_c = 2000$ K.

0.55 (close concentrations of the charged and neutral defects). In Fig. 8*b*, we fixed $E_a = 0.80$ eV, $E_b = 1.20$ eV, $T_c = 0$, but varied the fraction of charged defects: $w^+ = 0.10$ (solid line), $w^+ = 0.55$ (dashed line), $w^+ = 0.90$ (dash-dotted line). Now for a small fraction of charged defects ($w^+ = 0.10$), the *F* annealing, curve 2, is close to that for the neutral interstitials (curve 3). In the opposite case of predominant charged defects, $w^+ = 0.90$, the *F* annealing (curve 2″) becomes close to the curve 1″ for the charged interstitials. In both extreme cases the *F* annealing shows no distinctive step observed experimentally (see Fig. 7). Therefore, our conclusion about close initial concentrations of charged and neutral defects is true.

Lastly, let us consider Fig. 8*c* with the fixed set of parameters $E_a = 0.80$ eV, $E_b = 1.20$ eV, $w^+ = 0.55$, but variable Coulomb interaction: $T_c = 500$ K (solid line), $T_c = 1000$ K (dashed line), $T_c = 2000$ K (dash-dotted line). Now the kinetics for the *F* and F^+ centers split at low temperatures (around 600 K) and meet each other again at high temperatures (around 1000 K, when the Coulomb effects become negligible, see eq. (3)). Our estimate of the $T_c = 1000$ K [56,57] allows to reproduce very well the experimental data in Fig. 7.

5. Conclusions

A novel radiation defect with $S = 1/2$ has been found in neutron-irradiated α-Al_2O_3 single crystals (fluence of 6.9×10^{18} n/cm^2). Precise analysis of the EPR spectra in a range of 342-352 mT, their variation with magnetic field **B** rotation in different crystallographic planes and relevant parameters of the *g*-tensor ($g_z = 2.0459$, $g_y = 2.0049$ and $g_x = 2.0096$) allow us to conclude that a *single oxygen interstitial* has been experimentally revealed for the first time in metal oxides (see also our previous paper [32]). The revealed EPR signal belongs to a molecular type O_2^- center (known in chemistry as a superoxide ion) formed due to a chemical bonding of an oxygen interstitial, created during irradiation, with a regular oxygen ion and stabilized by a trapped hole. This hole-type O_2^- center occupies one regular anion site in the (0001) base plane of corundum, its molecular axis is oriented strictly along a bisectrix of the oxygen triangle (that coincide with one of three equivalent *a* crystal axes). The latter fact testifies that the O_2^- center is not associated with any spatially-close structural imperfection and can be considered as a single oxygen interstitial in a regular lattice region. The concentration of the O_2^- centers in our irradiated Al_2O_3 crystals equals 1×10^{18} cm^{-3} and is practically the same as for the F^+ centers. Note that the EPR-based configuration of an interstitial-containing defect has clearly been confirmed by the density functional theory calculations (see Ref. [32] for details).

The stepwise thermal annealing of Frenkel defects, the concentration of which has been estimated via the EPR signal intensity or integral of radiation-induced absorption bands (RIOA was decomposed into Gaussians each related to a certain defect type) has been performed exactly under the same conditions for both experimental methods. Based on excellent coincidence of annealing curves for the O_2^- center EPR signal and the RIOA Gaussian at 5.6 eV, we conclude that this elementary absorption band characterizes the same Frenkel defect, O_2^-. In contrast to earlier studied MgO and $MgAl_2O_4$ crystals [62,63]), the thermal annealing of the *F* and F^+ centers is a multistage process (with pronounced step at 750 K); in addition, there is an obvious high-temperature shift for the *F*-dependence.

These experimentally revealed features of the *F* and F^+ annealing kinetics have been thoroughly analyzed and explained in terms of interrelated diffusion-controlled recombination reactions between two pairs of Frenkel defects in different charge states (charged F^+, H^- and neutral *F*, H^0 centers). This analysis attributes the optical band peaked at 6.53 eV to the EPR-inactive neutral interstitials H^0, while the obtained interstitial migration energies coincide with those predicted in the quantum-chemical calculations [53,54].

CRediT authorship contribution statement

A. Lushchik: Conceptualization, Methodology, Investigation, Validation, Data curation, Writing – original draft, Visualization, Project administration. **V. Seeman:** Investigation, Validation, Data curation. **E. Shablonin:** Investigation, Validation, Visualization, Data curation. **E. Vasil'chenko:** Investigation, Validation, Data curation. **V.N. Kuzovkov:** Investigation, Validation, Data curation, Writing – review & editing. **E.A. Kotomin:** Conceptualization, Methodology, Investigation, Validation, Data curation, Writing – original draft, Project administration. **A.I. Popov:** Conceptualization, Methodology, Writing – review & editing.

Declaration of competing interest

The authors declare that they have no known competing financial interests or personal relationships that could have appeared to influence the work reported in this paper.

Acknowledgments

Authors are indebted to D. Gryaznov, A. Platonenko and R. Vila for valuable discussions. This work has been carried out within the framework of the EUROfusion Consortium, funded by the European Union via the Euratom Research and Training Programme (Grant Agreement No 101052200 — EUROfusion). Views and opinions expressed are however those of the authors only and do not necessarily reflect those of the European Union or the European Commission. Neither the European Union nor the European Commission can be held responsible for them. The research was partly (VK, EK and AP) performed in the Center of Excellence of the Institute of Solid State Physics, University of Latvia, supported through European Unions Horizon 2020 Framework Programme H2020-WIDESPREAD-01-2016-2017-TeamingPhase2 under grant agreement No. 739508, project CAMART^2.

References

[1] W.E. Lee, K.P.D. Lagerlof, Structural and electron diffraction data for sapphire (α-Al_2O_3), J. Electron. Microsc. Tech. 2 (1985) 247–258.
[2] T.H. Maiman, Stimulated optical radiation in ruby, Nature 187 (1960) 493–494.
[3] P.F. Moulton, Spectroscopic and laser characteristics of Ti:A1$_2$O$_3$, Opt. Soc. Am. B 3 (1986) 125–133.
[4] T.T. Basiev, S.B. Mirov, V.V. Osiko, Room-temperature color center lasers, IEEE J. Quant. Electron. 24 (1988) 1052–1069.
[5] M.S. Akselrod, V.S. Kortov, D.J. Kravetsky, V.I. Gotlib, Highly sensitive thermoluminescent anion-defective α-Al_2O_3:C single crystal detectors, Radiat. Protect. Dosim. 32 (1990) 15–20.
[6] S.W.S. McKeever, M.S. Akselrod, L.E. Colyott, N. Agersnap Larsen, J.C. Polf, V. H. Whitley, Characterisation of Al_2O_3 for use in thermally and optically stimulated luminescence dosimetry, Radiat. Protect. Dosim. 84 (1999) 163–168.
[7] S.M. Luca, N. Coron, C. Dujardin, H. Kraus, V.B. Mikhailik, M.-A. Verdier, P.C.F. Di Stefano, Scintillating and optical spectroscopy of Al_2O_3:Ti for dark matter searches, Nucl. Instrum. Methods A 606 (2009) 545–551.
[8] F.W. Clinard Jr., G.F. Hurley, L.W. Hobbs, Neutron irradiation damage in MgO, Al_2O_3 and $MgAl_2O_4$ ceramics, J. Nucl. Mater. 108–109 (1982) 655–670.
[9] G.P. Pells, Radiation damage effects in alumina, J. Am. Ceram. Soc. 77 (1994) 368–377.
[10] S.J. Zinkle, C. Kinoshita, Defect production in ceramics, J. Nucl. Mater. 251 (1997) 200–217.
[11] D.A. Blokhin, V.M. Chernov, I. Blokhin, Nuclear and physical properties of dielectrics under neutron irradiation in fast (BN-600) and fusion (DEMO-S) reactors, Phys. Atom. Nucl. 80 (2017) 1279–1284.
[12] S.M. Gonzales de Vicente, E.R. Hodgson, T. Shikama, Functional materials for tokamak in-vessel systems – status and applications, Nucl. Fusion 57 (2017), 092009.
[13] G.S. Was, D. Petti, S. Ukai, S. Zinkle, Materials for future nuclear energy systems, J. Nucl. Mater. 527 (2019), 151837.
[14] F.T. Gamble, R.H. Bartram, C.G. Young, O.R. Gilliam, P.W. Levy, Electron-spin resonance in gamma-ray- irradiated aluminium oxide, Phys. Rev. 134 (1964) A589–A595.
[15] F.T. Gamble, R.H. Bartram, C.G. Young, O.R. Gilliam, P.W. Levy, Electron-spin resonances in reactor-irradiated aluminium oxide, Phys. Rev. 138 (1965) A577–A583.
[16] S.Y. La, R.H. Bartram, R.T. Cox, The F^+ center in reactor-irradiated aluminum oxide, J. Phys. Chem. Solid. 34 (1973) 1079–1086.

[17] K.H. Lee, J.H. Crawford, Electron centers in single-crystal Al_2O_3, Phys. Rev. B 15 (1977) 4065–4070.
[18] J.H. Crawford Jr., Defects and defect processes in ionic oxides: where do we stand today? Nucl. Instrum. Methods B 1 (1984) 159–165.
[19] K. Atobe, N. Nishimoto, M. Nakagawa, Irradiation-induced aggregate centers in single crystal $A1_2O_3$, Phys. Status Solidi 89 (1985) 155–162.
[20] B.D. Evans, G.J. Pogatshnik, Y. Chen, Optical properties of lattice defects in α-Al_2O_3, Nucl. Instrum. Methods B 91 (1994) 258–262.
[21] B.D. Evans, A review of the optical properties of anion lattice vacancies, and electrical conduction in α-Al_2O_3: their relation to radiation-induced electrical degradation, J. Nucl. Mater. 219 (1995) 202–223.
[22] A.I. Surdo, V.S. Kortov, V.A. Pustovarov, Luminescence of F and F^+ centers in corundum upon excitation in the interval from 4 to 40 eV, Radiat. Meas. 33 (2001) 587–591.
[23] A. Seitbayev, V.A. Skuratov, A. Dauletbekova, YuG. Teterev, A.N. Krylov, M. Mamatova, M. Koloberdin, M. Zdorovets, Time-resolved high energy ionoluminescence of Al_2O_3, Nucl. Instrum. Methods B 500–501 (2021) 46–51.
[24] R. Ramírez, M. Tardío, R. Gonz_alez, J.E. Munoz Santiuste, M.R. Kokta, Optical properties of vacancies in thermochemically reduced Mg-doped sapphire single crystals, J. Appl. Phys. 101 (2007), 123520.
[25] A. Lushchik, Ch Lushchik, K. Schwartz, E. Vasil'chenko, T. Kärner, I. Kudryavtseva, V. Isakhanyan, A. Shugai, Stabilization and annealing of interstitials formed by radiation in binary metal oxides and fluorides, Nucl. Instrum. Methods B 266 (2008) 2868–2871.
[26] M. Izerrouken, T. Benyahia, Absorption and photoluminescence study of Al_2O_3 single crystal irradiated with fast neutrons, Nucl. Instrum. Methods B 468 (2010) 2987–2990.
[27] M. Izerrouken, Y. Djouadi, H. Zirour, Annealing process of F- and F^+-centers in Al_2O_3 single crystal induced by fast neutrons irradiation, Nucl. Instrum. Methods B 319 (2014) 29–33.
[28] V.S. Kortov, V.A. Pustovarov, S.V. Zvonarev, T.V. Shtang, Luminescence and radiation-induced color centers in anion-deficient alumina crystals after high-dose irradiation, Radiat. Meas. 90 (2016) 90–93.
[29] J.M. Costantini, Y. Watanabe, K. Yasuda, M. Fasoli, Cathodo-luminescence of color centers induced in sapphire and yttria-stabilized zirconia by high-energy electrons, J. Appl. Phys. 121 (2017), 153101.
[30] C. Grygiel, F. Moisy, M. Sall, H. Lebius, E. Balanzat, T. Madi, T. Been, D. Marie, I. Monnet, In-situ kinetics of modifications induced by swift heavy ions in Al_2O_3: colour centre formation, structural modification and amorphization, Acta Mater. 140 (2017) 157–167.
[31] A.I. Popov, A. Lushchik, E. Shablonin, E. Vasil'chenko, E.A. Kotomin, A. M. Moskina, V.N. Kuzovkov, Comparison of the F-type center thermal annealing in heavy-ion and neutron irradiated Al_2O_3 single crystals, Nucl. Instrum. Methods B 433 (2018) 93–97.
[32] V. Seeman, A. Lushchik, E. Shablonin, G. Prieditis, D. Gryaznov, A. Platonenko, E. A. Kotomin, A.I. Popov, Atomic, electronic and magnetic structure of an oxygen interstitial in neutron-irradiated Al_2O_3 single crystals, Sci. Rep. 10 (2020), 15852.
[33] E. Shablonin, A.I. Popov, G. Prieditis, E. Vasil'chenko, A. Lushchik, Thermal annealing and transformation of dimer *F* centers in neutron-irradiated Al_2O_3 single crystals, J. Nucl. Mater. 543 (2021), 152600.
[34] K. Nordlund, S.J. Zinkle, A.E. Sand, F. Granberg, R.S. Averback, R.E. Stoller, T. Suzudo, L. Malerba, F. Banhart, W.J. Weber, F. Willaime, S.L. Dudarev, D. Simeone, Primary radiation damage: a review of current understanding and models, J. Nucl. Mater. 512 (2018) 450–479.
[35] Ch Lushchik, A. Lushchik, Evolution of anion and cation excitons in alkali halide crystals, Phys. Solid State 60 (2018) 1487–1505, https://doi.org/10.1134/S1063783418080164.
[36] M. Kirm, G. Zimmerer E. Feldbach, A. Lushchik, Ch Lushchik, F. Savikhin, Self-trapping and multiplication of electronic excitations in Al_2O_3 and Al_2O_3:Sc crystals, Phys. Rev. B 60 (1999) 502–510.
[37] N. Itoh, D.M. Duffy, S. Khakshouri, A.M. Stoneham, Making tracks: electronic excitation roles in forming swift heavy ion tracks, J. Phys. Condens. Matter 21 (2009), 474205.
[38] A. Lushchik, T. Kärner, Ch Lushchik, K. Schwartz, F. Savikhin, E. Shablonin, A. Shugai, E. Vasil'chenko, Electronic excitations and defect creation in wide-gap MgO and $Lu_3Al_5O_{12}$ crystals irradiated with swift heavy ions, Nucl. Instrum. Methods B 286 (2012) 200–208.
[39] M. Toulemonde, W. Assmann, C. Dufour, A. Meftah, C. Trautmann, Nanometric transformation of the matter by short and intense electronic excitation: experimental data versus inelastic thermal spike model, Nucl. Instrum. Methods B 277 (2012) 28–39.
[40] A. Lushchik, Ch Lushchik, K. Schwartz, F. Savikhin, E. Shablonin, A. Shugai, E. Vasil'chenko, Creation and clustering of Frenkel defects at high density of electronic excitations in wide-gap materials, Nucl. Instrum. Methods B 277 (2012) 40–44.
[41] E. Ion beam modification of solids, in: W. Wesch, E. Wendler (Eds.), Springer Series in Surface Sciences, vol. 61, Springer Nature, 2016.
[42] K.H. Lee, J.H. Crawford, Additive coloration of sapphire, Appl. Phys. Lett. 33 (1978) 273–275.
[43] L.E. Halliburton, L.A. Kappers, (Radiation-induced oxygen interstitials in MgO, Solid State Commun. 26 (1978) 111–114.
[44] D. Schoemaker, Games people play with interstitials (in alkali halides), J. Phys. Colloq. 37 C7 (1976). C7-, 63, C, C7-71.
[45] J.H. Lunsford, J.P. Jayne, Electron paramagnetic resonance of oxygen on ZnO and ultraviolet-irradiated MgO, J. Chem. Phys. 44 (1966) 1487–1492.
[46] T. Kärner, S. Dolgov, N. Mironova-Ulmane, S. Nakonechnyi, E. Vasil'chenko, Anion interstitials in neutron-irradiated MgO single crystals, Radiat. Meas. 33 (2001) 625–628.
[47] T.P.P. Hall, Studies of neutron irradiation damage in CaO: I, J. Phys. C Solid State Phys. 8 (1975) 1921–1927.
[48] M. Che, A.J. Tench, S. Colluccia, A. Zecchina, Pyridine-induced formation of $^{17}O_2^-$-adsorbed on thermally activated CaO, J. Chem. Soc. Faraday Trans. I 72 (1976) 1553–1558.
[49] Y. Ono, H. Takagava, S. Fukuzumi, On the formation of O_2^- ion on calcium oxide, Z. Phys. Chem. Neue Fol. 115 (1979) 51–54.
[50] V. Seeman, S. Reifman, T. Lehto, Ü. Haldre, Family of O_2^- centers in SrO crystals, Phys. Status Solidi B 102 (1980) 459–465.
[51] R.C. Barklie, J.R. Niklas, J.M. Spaeth, ENDOR measurements of defects in sodium ß-alumina. I, J. Phys. C Solid State Phys. 13 (1980) 1745–1755.
[52] T. Brudevoll, E.A. Kotomin, N.E. Christensen, Interstitial oxygen atom diffusion in MgO, Phys. Rev. B 53 (1996) 7731–7735.
[53] YuF. Zhukovskii, A. Platonenko, S. Piskunov, E.A. Kotomin, Ab initio simulations on migration paths of interstitial oxygen in corundum, Nucl. Instrum. Methods B 374 (2016) 29–34.
[54] A. Platonenko, D. Gryaznov, Y.F. Zhukovskii, E.A. Kotomin, Ab initio simulations on charged interstitial oxygen migration in corundum, Nucl. Instrum. Methods B 435 (2018) 74–78.
[55] E. Kotomin, V. Kuzovkov, A.I. Popov, J. Maier, R. Vila, Anomalous kinetics of diffusion-controlled annealing of the F-type centers in irradiated ionic solids, J. Phys. Chem. 122 (2018) 28–32.
[56] A. Lushchik, V.N. Kuzovkov, A.I. Popov, G. Prieditis, V. Seeman, E. Shablonin, E. Vasil'chenko, E.A. Kotomin, Evidence for the formation of two types of oxygen interstitials in neutron-irradiated α-Al_2O_3 single crystals, Sci. Rep. 11 (2021), 20909.
[57] A. Lushchik, V.N. Kuzovkov, I. Kudryavtseva, A.I. Popov, V. Seeman, E. Shablonin, E. Vasil'chenko, E.A. Kotomin, The two types of oxygen interstitials in neutron-irradiated corundum single crystals: joint experimental and theoretical study, Phys. Status Solidi B (2021), 2100317, https://doi.org/10.1002/pssb.202100317.
[58] A. Lushchik, S. Dolgov, E. Feldbach, R. Pareja, A.I. Popov, E. Shablonin, V. Seeman, Creation and thermal annealing of structural defects in neutron-irradiated $MgAl_2O_4$ single crystals, Nucl. Instrum. Methods B 435 (2018) 31–37.
[59] V. Seeman, E. Feldbach, T. Kärner, A. Maaroos, N. Mironova-Ulmane, A.I. Popov, E. Shablonin, E. Vasil'chenko, A. Lushchik, Fast-neutron-induced and as-grown structural defects in magnesium aluminate spinel crystals with different stoichiometry, Opt. Mater. 91 (2019) 42–49.
[60] V.N. Kuzovkov, A.I. Popov, E.A. Kotomin, A.M. Moskina, E. Vasil'chenko, A. Lushchik, Theoretical analysis of the kinetics of low-temperature defect recombination in alkali halide crystals, Low Temp. Phys. 42 (2016) 588–593, https://doi.org/10.1063/1.4959018.
[61] E.A. Kotomin, V. N Kuzovkov, A.I. Popov, R. Vila, Kinetics of F center annealing and colloid formation in Al_2O_3, Nucl. Instrum. Methods B 374 (2016) 107–110.
[62] G. Baubekova, A. Akilbekov, E.A. Kotomin, V.N. Kuzovkov, A.I. Popov, E. Shablonin, M. Zdorovets, E. Vasil'chenko, A. Lushchik, Thermal annealing of radiation damage caused by swift ^{132}Xe ions in MgO single crystals, Nucl. Instrum. Methods B 462 (2020) 163–168.
[63] A. Lushchik, E. Feldbach, E.A. Kotomin, I. Kudryavtseva, V.N. Kuzovkov, A. I. Popov, V. Seeman, E. Shablonin, Distinctive features of diffusion-controlled radiation defect recombination in stoichiometric magnesium aluminate spinel crystals and transparent polycrystalline ceramics, Sci. Rep. 10 (2020) 7810.
[64] J.A. Weil, J.R. Bolton, J.E. Wertz, Electron Paramagnetic Resonance: Elementary Theory and Applications, Wiley-interscience, New York, 1994, p. 89.
[65] www.easyspin.org.
[66] R.T. Cox, Electron spin resonance of holes trapped at Mg^{2+}, Li^+ and cation vacancies in Al_2O_3, Solid State Commun. 9 (1971) 1989–1992.
[67] K.H. Lee, G.E. Holmberg, J.H. Crawford Jr., Hole centers in γ-irradiated, oxidized Al_2O_3, Solid State Commun. 20 (1976) 183–185.
[68] K.H. Lee, G.E. Holmberg, J.H. Crawford Jr., Optical and ESR studies of hole centers in γ-irradiated Al_2O_3, Phys. Status Solidi 39 (1977) 669–674.
[69] F.J. Adrian, A.N. Jette, J.M. Spaeth, Theory of indirect hyperfine interactions of oxygen-aluminum defects in ionic crystals, Phys. Rev. B 31 (1985) 3923–3931.
[70] S. Dolgov, T. Kärner, A. Lushchik, A. Maaroos, S. Nakonechnyi, E. Shablonin, Trapped-hole centers in MgO single crystals, Phys. Solid State 53 (2011) 1244.
[71] Y. Chen, M.M. Abraham, Trapped-hole centers in alkaline-earth oxides, J. Phys. Chem. Solid. 51 (1990) 747–764.
[72] N. Itoh, Interstitial and trapped-hole centers in alkali halides, Cryst. Lattice Defects 3 (1972) 113–143.
[73] S. Radhakrishna, V.R. Chowdari, Radiation damage products in ionic crystals. Impurity doped alkali halides, Fortschr. Phys. 25 (1977) 511–678.
[74] Ch Lushchik, J. Kolk, A. Lushchik, N. Lushchik, M. Tajirov, E. Vasil'chenko, Decay of excitons into long-lived F,H and α,I pairs in KCl, Phys. Status Solidi B 114 (1982) 103–111.
[75] A.Ch Lushchik, A.G. Frorip, Thermalized and hot interstitial halogen ions in alkali halides, Phys. Status Solidi B 161 (1990) 525–535.
[76] T.P. P Hall, Studies of neutron irradiation damage in CaO: II, J. Phys. C Solid State Phys. 9 (1976) 1369–1379.
[77] B. Henderson, Optical pumping cycle of exchange-coupled F^+-centre pairs in MgO and CaO, J. Phys. C Solid State Phys. 9 (1976) 2185–2195.
[78] T.R. Waite, General theory of bimolecular reaction rates in solids and liquids, J. Chem. Phys. 28 (1958) 103–106.

[79] E.A. Kotomin, V.N. Kuzovkov, Phenomenological kinetics of Frenkel defect recombination and accumulation in ionic solids, Rep. Prog. Phys. 55 (1992) 2079–2188.
[80] M.V. Smoluchowski, Versuch einer mathematischen theorie der Koagulationskinetik kolloider losungen, Z. Phys. Chem. B 92 (1917) 129–168.
[81] P. Debye, Reaction rates in ionic solutions, Trans. Electrochem. Soc. 82 (1942) 265–272.